PERGAMON

International Journal of Solids and Structures 40 (2003) 4003–4019

INTERNATIONAL JOURNAL OF SOLIDS and STRUCTURES

www.elsevier.com/locate/ijsolstr

Description of inelastic behaviour of structural masonry

S. Pietruszczak *, R. Ushaksaraei

Department of Civil Engineering, McMaster University, 1280 Main St. West, Hamilton, Ont., Canada L8S 4L7

Received 16 July 2002; received in revised form 11 March 2003

Abstract

The focus of this paper is on the description of progressive failure in structural masonry. A continuum formulation is developed here applicable to a representative volume which comprises a large number of units interspersed by mortar joints. The conditions at failure are defined by employing a critical plane approach, whereby the orientation of the localization plane is specified by solving a constrained optimization problem. The framework is subsequently extended to model the inelastic deformation process. This is accomplished by incorporating a multi-laminate approach in which the average response is derived from sliding/separation characteristics along a set of randomly distributed planes. The localized deformation is described by considering a structured medium comprising the intact masonry intercepted by a distinct macrocrack. Extensive numerical simulations are performed examining the response of brickwork in compression/tension regimes, at different orientations of the bed joints relative to the loading direction. A boundary-value problem is also studied involving an inelastic finite element analysis of a bearing masonry wall subjected to in-plane loading.

Keywords: Structural masonry; Plasticity; Homogenization; Anisotropy; Finite element analysis

1. Introduction

Finite element analysis of large masonry structures cannot, in general, be conducted by discretizing individual units and/or mortar joints, as this would be computationally prohibitive. Therefore, some macroscopic formulations should be employed, which are capable of describing the anisotropic properties of the brickwork. In recent years, several attempts have been made to estimate the average properties of masonry panels. Those include micropolar Cosserat continuum models (e.g., Sulem and Muhlhaus, 1997; Masiani and Trovalusci, 1996) as well as applications of the mathematical theories of homogenization for periodic media (e.g., Anthoine, 1995, 1997; Urbanski et al., 1995). Such approaches, although rigorous, have never been implemented in the context of a structural analysis of practical engineering problems. For Cosserat media, one of the main difficulties is the development of a systematic methodology for identification of equivalent continuum properties. For a rigorous homogenization approach, the extension to

* Corresponding author. Tel.: +1-905-525-9140; fax: +1-905-529-9688.
E-mail address: pietrusz@mcmaster.ca (S. Pietruszczak).

0020-7683/03/$ - see front matter © 2003 Elsevier Science Ltd. All rights reserved.
doi:10.1016/S0020-7683(03)00174-4

inelastic range poses profound conceptual problems and is not, in general, feasible. Given these difficulties, a number of simplified approaches have been developed incorporating various idealizations at the level of either the geometry of brickwork or the interaction between the constituents. Such approximate homogenization techniques include the works of Pande et al. (1989), Maier et al. (1991), Lourenco and Zucchini (2001), etc. However, even for these simplified models, the implementation in the context of a non-linear finite element analysis is still a difficult task and has not yet been accomplished.

The main objective of this work is to develop a continuum theory for describing the inelastic behaviour of structural masonry. The approach may be perceived as a pragmatic alternative to the homogenization method. It is simpler in numerical implementation and addresses all stages of the deformation process, including the localized deformation associated with formation of macrocracks.

The paper is written in the following sequence. In the next section, a general formulation of the problem is provided. The conditions at failure are described by invoking a critical plane approach. Here, the failure criterion is defined in terms of traction components acting on a physical plane and its representation employs a set of distribution functions specifying the variation of strength parameters. The approach consists of finding such an orientation of the localization plane for which the failure function reaches a maximum. This approach is subsequently extended to incorporate the inelastic deformation. The behaviour along each plane is defined in terms of a plasticity framework and the global macroscopic response is obtained by averaging the contributions from all active planes. The formation of macrocracks is perceived as a localization problem and the formulation is derived by incorporating a volume averaging procedure which employs a 'characteristic dimension'. The general mathematical framework is illustrated by some numerical examples provided in Section 3. Here, the details pertaining to the specification of material functions/parameters are discussed first, followed by numerical analyses examining the response of brickwork in compression and tension regimes for different orientations of the bed joints. The paper is concluded by presenting the results of a finite element analysis of a bearing masonry wall subjected to in-plane loading. Here, the evolution of the crack pattern is investigated, prior to the collapse of the wall, and a simple reinforcement strategy is examined.

2. General formulation

In this section, a mathematical model describing the inelastic response of structural masonry is outlined. Fig. 1 shows a schematic diagram of a representative volume of the material, which consists of a large number of masonry units interspersed by two orthogonal families of bed and head joints filled with mortar. The geometry of the problem is referred to a coordinate system $\boldsymbol{x}$, while the principal material triad is defined by the base vectors $\boldsymbol{l}^{(1)}$, $\boldsymbol{l}^{(2)}$, $\boldsymbol{l}^{(3)}$. The general formulation of the problem comprises three main aspects. The first one is related to specification of the conditions at failure, which is accomplished by incorporating a critical plane approach. The second step involves an extension of this approach to model the inelastic deformation. This is achieved by incorporating a plasticity framework, in which the response is described in terms of sliding/separation along a set of randomly distributed planes. The last issue involves the description of localized deformation associated with formation of macrocracks.

2.1. Failure locus for structural masonry

The conditions at failure can be defined by postulating a path-independent criterion. The general form of the failure function incorporated here is similar to that proposed in a recent article by Ushaksaraei and Pietruszczak (2002). The formulation of the problem is based on a critical plane approach (Pietruszczak and Mroz, 2001), which consists of specifying the orientation of a localization plane on which the failure

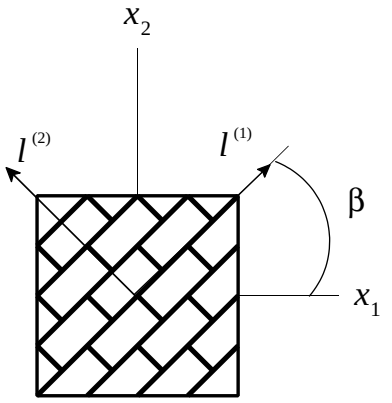

Fig. 1. Geometry of the problem.

function reaches a maximum. In this section, the main assumptions embedded in this criterion are briefly reviewed.

For a representative volume as depicted in Fig. 1, the conditions at failure along an arbitrary plane of orientation n_i, are defined here by invoking a simple bi-linear representation

$$\begin{aligned} &F(n_i) = \tau + \mu^{c}\sigma - c = 0; \quad \text{for } \sigma \leqslant 0 \\ &F(n_i) = \tau - c(1 - \sigma/\sigma_0) = 0; \quad \text{for } \sigma > 0 \end{aligned} \tag{1}$$

In the expressions above, τ and σ are the shear and normal components of the traction vector, t_i, on this plane, i.e.

$$\tau = |\sigma_{ij} n_i s_j|, \quad \sigma = \sigma_{ij} n_i n_j \tag{2}$$

where

$$s_i = t_i^s / \|t_i^s\|, \quad t_i^s = (\delta_{ij} - n_i n_j)\sigma_{jk} n_k; \quad n_i s_i = 0 \tag{3}$$

Moreover, the parameters μ^{c} and c represent the coefficient of friction and cohesion, respectively, whereas σ_0 denotes the tensile strength in the direction normal to the plane. Eq. (1) may be perceived as a simple approximation to a more general quadratic form, as considered in the original reference. The geometric representation of the failure criterion (1) is provided in Fig. 2.

In order to describe the anisotropic nature of the structural masonry, all the basic material parameters have been defined in terms of distribution functions

$$\begin{aligned} &\mu^{c} = \mu_{o}^{c}(1 + \Omega_{ij}^{\mu} n_i n_j), \quad c = c_{01}(1 + \Omega_{ij}^{c} n_i n_j) + c_{02}(\Omega_{ij}^{c} n_i n_j)^2 \\ &\sigma_0 = \sigma_{01}(1 + \Omega_{ij}^{\sigma} n_i n_j) + \sigma_{02}(\Omega_{ij}^{\sigma} n_i n_j)^2 \end{aligned} \tag{4}$$

In Eq. (4), μ_{o}^{c} designates the orientation average of μ^{c}; σ_{01}, σ_{02} and c_{01}, c_{02} are constants, whereas Ω's represent a set of symmetric traceless tensors which describe the bias in the spatial distribution of the parameters. It is noted that the distribution of c and σ_0 employs second-order dyadic products of Ω_{ij} and $n_i n_j$, which allows for a more accurate representation of the material behaviour.

The orientation of the localization plane can be determined by maximizing the failure function F, Eq. (1), with respect to n_i and s_i, subject to constraints $n_i n_i = 1$, $s_i s_i = 1$, $n_i s_i = 0$. Introducing Lagrange multipliers λ_1, λ_2, λ_3, the corresponding Lagrangian functions become

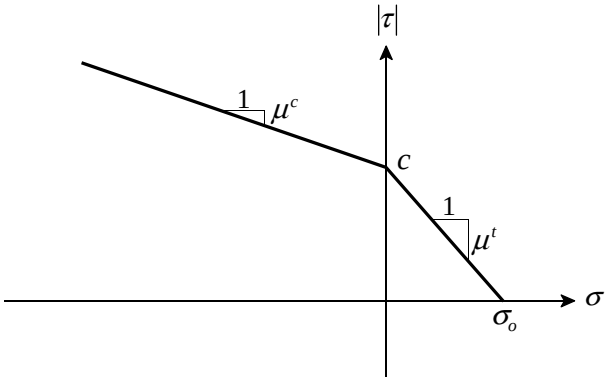

Fig. 2. Failure criterion on an arbitrarily oriented plane.

$$G = |\sigma_{ij} n_i s_j| + \mu_o^c (1 + \Omega_{ij}^{\mu} n_i n_j)\sigma_{pq} n_p n_q - c_{01}(1 + \Omega_{ij}^{c} n_i n_j) - c_{02}(\Omega_{ij}^{c} n_i n_j)^2 - \lambda_1 (n_i n_i - 1) - \lambda_2 (s_i s_i - 1) - \lambda_3 n_i s_i \tag{5}$$

for $\sigma \leqslant 0$, and

$$G = |\sigma_{ij} n_i s_j|[\sigma_{01}(1 + \Omega_{ij}^{\sigma} n_i n_j) + \sigma_{02}(\Omega_{ij}^{\sigma} n_i n_j)^2] - [c_{01}(1 + \Omega_{ij}^{c} n_i n_j) + c_{02}(\Omega_{ij}^{c} n_i n_j)^2][\sigma_{01}(1 + \Omega_{pq}^{\sigma} n_p n_q) + \sigma_{02}(\Omega_{pq}^{\sigma} n_p n_q)^2 - \sigma_{pq} n_p n_q] - \lambda_1 (n_i n_i - 1) - \lambda_2 (s_i s_i - 1) - \lambda_3 n_i s_i \tag{6}$$

for $\sigma > 0$.

The stationary conditions with respect to n_i and s_i, together with the constraints of the problem, provide now a set of algebraic equations which can be solved to define the orientation of the localization plane along which F is a maximum.

2.2. Description of inelastic deformation

In this part, the methodology outlined above is extended to incorporate the description of the deformation process. This is accomplished by attributing the inelastic behaviour to sliding/separation along an infinite set of randomly oriented planes. For each plane, the conditions at failure are represented by the local criterion (1), which incorporates the scalar–valued functions (4). The inelastic deformation is then accounted for by invoking an appropriate plasticity formulation. This approach is conceptually similar to the so-called multi-laminate framework (Pande and Sharma, 1983; Pietruszczak and Pande, 1987).

Assume that the yield and plastic potential functions for the ith plane, with unit normal n_i, have a general form

$$f(n_i) = f(\sigma, \tau, \kappa) = 0; \quad \psi(n_i) = \psi(\sigma, \tau) = \text{const.} \tag{7}$$

where τ and σ are defined according to Eq. (2) and κ is a hardening parameter, which is a function of the plastic deformation history. The equation of the yield surface is formulated in such a way that $\kappa \to \infty \Rightarrow F \to 0$, so that the conditions at failure are consistent with the representation (1).

Introducing a local frame $\bar{\boldsymbol{x}}$ associated with the base vectors n_i and s_i, the flow rule may be written as

$$\dot{\bar{e}}_i^p = \dot{\lambda} \frac{\partial \psi}{\partial \bar{t}_i} \tag{8}$$

where $\bar{e}_i$ is the strain vector, whereas the corresponding traction $\bar{t}_i$ has the components $\bar{t}_i = \{\sigma, \tau, 0\}$. The strain rates contributed by this plane are expressed as a symmetric part of a dyadic product

$$\dot{\varepsilon}^p_{ij} = \tfrac{1}{2}(\dot{e}^p_i n_j + \dot{e}^p_j n_i); \quad \dot{e}^p_i = T_{ij}\dot{\bar{e}}^p_j \tag{9}$$

where T_{ij} is the transformation matrix. Thus, substituting (8) into (9)

$$\dot{\varepsilon}^p_{ij} = \frac{1}{2}\dot{\lambda}(T_{ip}n_j + T_{jp}n_i)\frac{\partial \psi}{\partial \bar{t}_p} \tag{10}$$

The global macroscopic deformation is obtained by averaging the contributions from all active planes. Thus,

$$\dot{\underset{\sim}{\varepsilon}}^p_{ij} = \frac{1}{8\pi}\int_S \dot{\lambda}(T_{ip}n_j + T_{jp}n_i)\frac{\partial \psi}{\partial \bar{t}_p}\,\mathrm{d}S \tag{11}$$

In practical implementations, the integration process is carried out numerically by adopting a set of 'sampling planes'. Details concerning the orientation of these planes and the distribution of weight coefficients are provided by Pande and Sharma (1983).

The global constitutive relation may now be obtained by invoking the additivity of elastic and plastic deformation, i.e.

$$\dot{\varepsilon}_{ij} = C_{ijkl}\dot{\sigma}_{kl} + \dot{\underset{\sim}{\varepsilon}}^p_{ij} \tag{12}$$

where C_{ijkl} is the elastic compliance operator. It is noted that this operator may be estimated by invoking a homogenization technique. Several such approaches have been reported in the literature (e.g., Anthoine, 1995; Pietruszczak and Niu, 1992; Pande et al., 1989).

2.3. Description of localized deformation

The constitutive relation (12) governs the response of the material prior to the onset of a localized deformation mode, which is associated with formation of macrocracks. Within the framework employed here, the localization takes place on a plane for which $F = \max F$ and the direction of the macrocrack is identified with that of the critical plane. The behaviour after the inception of localization is described by incorporating an averaging procedure, similar to that developed in Pietruszczak (1999).

Referring to Fig. 3, consider a representative volume of the material, which comprises now the 'intact' masonry intercepted by a macrocrack of a given orientation $\hat{n}_i$. The formulation of the problem incorporates the stress/strain rate decomposition based on volume averaging

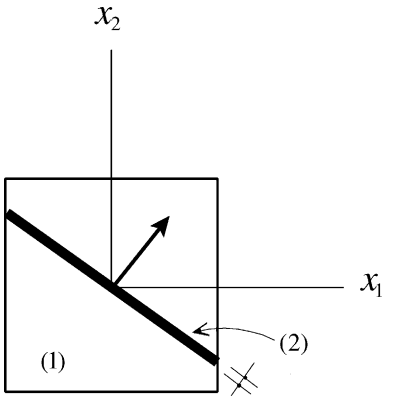

Fig. 3. Sample intercepted by a macrocrack of orientation $\hat{n}_i$.

$$\dot{\boldsymbol{\sigma}}_{ij} = \upsilon^{(1)}\dot{\boldsymbol{\sigma}}_{ij}^{(1)} + \upsilon^{(2)}\dot{\boldsymbol{\sigma}}_{ij}^{(2)}; \quad \dot{\boldsymbol{\varepsilon}}_{ij} = \upsilon^{(1)}\dot{\boldsymbol{\varepsilon}}_{ij}^{(1)} + \upsilon^{(2)}\dot{\boldsymbol{\varepsilon}}_{ij}^{(2)} \tag{13}$$

Here, the index (1) refers to the intact material outside the localization zone, (2) denotes the material in the fractured zone and υ's represent the corresponding volume fractions. All quantities are referred to the global coordinate system. The strain rate in the fractured zone may be conveniently defined in terms of velocity discontinuities $\dot{\boldsymbol{g}}_i$, as a symmetric part of a dyadic product

$$\dot{\boldsymbol{\varepsilon}}_{ij}^{(2)} = \frac{1}{2h}(\dot{\boldsymbol{g}}_i\hat{\boldsymbol{n}}_j + \dot{\boldsymbol{g}}_j\hat{\boldsymbol{n}}_i) \tag{14}$$

where h is the thickness of the macrocrack.

The equilibrium requires that the traction t_i along the discontinuity plane remains continuous. Thus,

$$\dot{\boldsymbol{t}}_i = \dot{\boldsymbol{\sigma}}_{ij}^{(1)}\hat{\boldsymbol{n}}_j \tag{15}$$

Assume now the constitutive relations for both constituents take the general form

$$\dot{\boldsymbol{\varepsilon}}_{ij}^{(1)} = C_{ijkl}\dot{\boldsymbol{\sigma}}_{kl}^{(1)}; \quad \dot{\boldsymbol{g}}_i = K_{ij}\dot{\boldsymbol{t}}_j \tag{16}$$

It should be noted that since the material in the fractured zone undergoes strain–softening, C_{ijkl} is, in general, an elastic operator as defined by Eq. (12). Substituting now the second relation in Eq. (16) into Eq. (14), and taking into account Eq. (15) gives

$$\dot{\boldsymbol{\varepsilon}}_{ij}^{(2)} = \frac{1}{2h}(K_{ip}\hat{\boldsymbol{n}}_j\hat{\boldsymbol{n}}_k + K_{jp}\hat{\boldsymbol{n}}_i\hat{\boldsymbol{n}}_k)\dot{\boldsymbol{\sigma}}_{pk}^{(1)} \tag{17}$$

Thus, in view of the strain decomposition (13)

$$\dot{\boldsymbol{\varepsilon}}_{ij} = \upsilon^{(1)}C_{ijkl}\dot{\boldsymbol{\sigma}}_{kl}^{(1)} + \tfrac{1}{2}\upsilon(K_{ip}\hat{\boldsymbol{n}}_j\hat{\boldsymbol{n}}_k + K_{jp}\hat{\boldsymbol{n}}_i\hat{\boldsymbol{n}}_k)\dot{\boldsymbol{\sigma}}_{pk}^{(1)} \tag{18}$$

where $\upsilon = \upsilon^{(2)}/h$ represents the ratio of the area of the fractured zone to the volume of the sample. Thus the parameter υ is, in fact, independent of h. Noting now that $\upsilon^{(2)} \ll \upsilon^{(1)}$, the stress decomposition in Eq. (13) simplifies to $\dot{\boldsymbol{\sigma}}_{ij} \simeq \upsilon^{(1)}\dot{\boldsymbol{\sigma}}_{ij}^{(1)} \simeq \dot{\boldsymbol{\sigma}}_{ij}^{(1)}$. Therefore, Eq. (18) can be approximated by

$$\dot{\boldsymbol{\varepsilon}}_{ij} = [C_{ijpk} + \tfrac{1}{2}\upsilon(K_{ip}\hat{\boldsymbol{n}}_j\hat{\boldsymbol{n}}_k + K_{jp}\hat{\boldsymbol{n}}_i\hat{\boldsymbol{n}}_k)]\dot{\boldsymbol{\sigma}}_{pk} \tag{19}$$

which provides the required macroscopic constitutive relation.

3. Numerical simulations

In this section, the constitutive relations formulated above have been implemented in a numerical code in order to investigate the response of structural masonry panels in a series of axial compression/tension tests. The simulations have been carried out for different orientations of the bed joints relative to the loading direction. Whenever possible, the predictions have been compared with the experimental data reported in the literature. In what follows, the details on the specification of material functions are discussed first; later, the results of the numerical simulations are presented.

3.1. Specification of material functions

The inelastic deformation process has been described by invoking the framework presented in the preceding Section 2.2. A simple formulation has been implemented here, whereby the irreversible deformations in the tensile regime, prior to formation of a macrocrack, have been neglected. Consequently, the

yield condition for $\sigma > 0$ has been assumed in the same functional form as the second equation in (1), while in the compression regime, a linear approximation has been employed

$$f(n_i) = \tau + \mu\sigma - c = 0; \quad \mu = \mu(\kappa) \tag{20}$$

where κ is a hardening parameter. The hardening effects have been attributed here to the plastic shear strain, i.e.

$$\mu = \mu^{\mathrm{c}} \frac{\kappa}{A + \kappa}; \quad \kappa = \int |\dot{\gamma}^p| \, \mathrm{d}t \tag{21}$$

where $\dot{\gamma}^p = \dot{\tilde{e}}_2^p$ and A is a material constant. It should be noted that, according to Eq. (21), as $\kappa \to \infty$ there is $\mu \to \mu^{\mathrm{c}}$ which implies that $f(n_i) \to F(n_i)$. Thus, the conditions at failure are consistent with those stipulated by the first equation in (1).

The plastic flow has been described by a non-associated rule, Eq. (8), in which the potential function has been defined as

$$\psi(n_i) = \tau - \eta_{\mathrm{c}}(\sigma - \sigma_0^{\mathrm{c}}) \ln \frac{\sigma_0^{\mathrm{c}} - \sigma}{\hat{\sigma}_0} = 0; \quad \sigma_0^{\mathrm{c}} = \frac{c}{\mu^{\mathrm{c}}} \tag{22}$$

Here, $\hat{\sigma}_0$ is evaluated from the condition $\psi(n_i) = 0$, whereas η_{c} is a parameter which represents the value of $\eta = \tau/(\sigma_0^{\mathrm{c}} - \sigma)$ at which a transition from compaction to dilatancy takes place.

The above description, viz. Eqs. (20)–(22), is rather simplistic and apparently other, more elaborated plasticity frameworks can be implemented here. In particular, the formulation may be augmented by accounting for sensitivity of the hardening characteristics to the value of the normal component of the traction as well as incorporating the inelastic behaviour in the tensile regime.

Finally, it is noted that the elastic properties associated with each sampling plane can be defined by invoking the dyadic decomposition in Eq. (9). Thus,

$$t_i = \sigma_{ij} n_j = A_{ij} e_j; \quad A_{ij} = D_{ijkl} n_j n_k \tag{23}$$

where $D_{ijkl} = C_{ijkl}^{-1}$ is the elastic stiffness operator, which has been estimated here based on a homogenization procedure described in Pietruszczak and Niu (1992).

The strain localizes on a 'critical' plane, for which the value of the failure function $F(n_i)$ is maximum. The description of the localized deformation requires the specification of the operator K_{ij}, Eq. (16), which defines the properties of the material confined to the fracture zone. These properties have been described here by invoking again a simple plasticity framework, which incorporates a strain–softening. It is noted that the stress state at the inception of localization satisfies $F \to 0$, where the function F is defined in Eq. (1). Substituting in both these equations $c = \mu^{\mathrm{t}}\sigma_0$, where μ^{t} is the slope of the tensile branch (Fig. 2), one obtains

$$F(n_i) = \tau + \mu\sigma - \mu^{\mathrm{t}}\sigma_0 = 0 \tag{24}$$

where $\mu = \mu^{\mathrm{t}}$ for $\sigma > 0$ (tension regime) and $\mu \to \mu^{\mathrm{c}}$ for $\sigma \leqslant 0$ (in compression). Thus, the yield function associated with the localization plane, has been chosen in a functional form consistent with representation (24), i.e.

$$f(\hat{n}_i) = \tau + \mu\sigma - \mu^{\mathrm{t}}\overline{\sigma}_0 = 0 \tag{25}$$

where $\hat{n}_i$ specifies the normal to the localization plane, $\overline{\sigma}_0$ is the softening function and $\mu = \text{const.}$ is evaluated at the onset of localization.

The strain–softening effects have been attributed to the normal component of the displacement discontinuity g_1^p and the degradation function $\overline{\sigma}_0 = \overline{\sigma}_0(\kappa)$ has been selected in a simple exponential form

$$\overline{\sigma}_0 = \sigma_0 \, \mathrm{e}^{-C\kappa}; \quad \kappa = \int |\dot{g}_1^p| \, \mathrm{d}t \tag{26}$$

where σ_0 is the tensile strength in the direction normal to the localization plane and C represents a material constant. The formulation incorporated an associated flow rule, which in the context of Eq. (25), resulted in a progressive dilation in the fractured zone. Given Eqs. (25) and (26), the operator K_{ij} can be easily established following a standard plasticity formalism.

Finally, note that after the inception of strain localization, the material response is sensitive to the 'characteristic dimension' υ, which appears in the constitutive relation (19). In the numerical simulations carried out under Section 3.2, the value of υ was evaluated based on the geometry of the brickwork panel and the corresponding orientation of the localization plane. In the context of finite element analysis, as presented in Section 4, υ was estimated by evaluating a partitioned volume associated with each Gauss point, in a manner similar to that as described in Pietruszczak and Niu (1992).

3.2. Numerical results

The formulation of the problem, as presented above, incorporates a number of material parameters which need to be identified. Those include, in addition to elastic constants, a set of parameters defining the conditions at failure, i.e. those appearing in the distribution functions (4); the parameters A and η_c, Eqs. (21) and (22), governing the inelastic behaviour on the ith plane; and the constant C, Eq. (26), specifying the rate of softening associated with the localized deformation.

The functions specified in Eq. (4) have been selected based on the experimental data reported by Page (1983). Note that the set of functions employed here, is somewhat different from that adopted in Ushaksaraei and Pietruszczak (2002). In particular, the latter reference incorporated μ^t, Eq. (24), rather than cohesion c, Eq. (1), as an independent variable. The current choice is motivated primarily by simplifications in the identification procedure, whereby the properties in tension do not explicitly affect those in compression. The details on the identification procedure for $\sigma_0(n_i)$, $\mu^c(n_i)$ and $\mu^t(n_i)$ are provided in Ushaksaraei and Pietruszczak (2002). Here, a quadratic approximation has been employed for $\sigma_0(n_i)$, while the key-values of $c(n_i)$ have been estimated from the respective distributions of $\sigma_0(n_i)$ and $\mu^t(n_i)$ provided in the earlier reference. Furthermore, the functions (4) have been augmented to include orthotropic characteristics. It is noted that no experimental data is available in Page (1983) on the out-of-plane properties. Therefore, the latter have been assessed on a rather intuitive basis, following again the procedure analogous to that set out in Ushaksaraei and Pietruszczak (2002). The corresponding values of the material parameters are:

$$\Omega_1^{\mu^c} = \Omega_2^{\mu^c} = 0; \quad \sigma_{01} = 0.898 \text{ MPa}; \quad \sigma_{02} = -14.249 \text{ MPa}; \quad \Omega_1^{\sigma} = -0.158;$$
$$\Omega_2^{\sigma} = 0.249; \quad c_{01} = 2.498 \text{ MPa}; \quad c_{02} = -19.281 \text{ MPa}; \quad \Omega_1^{c} = -0.221; \quad \Omega_2^{c} = 0.393$$

The elastic properties of the brickwork can, in general, be estimated by invoking a homogenization procedure. In the numerical simulations presented here, the values of elastic constants have been chosen based on the estimates developed in the article by Pietruszczak and Niu (1992). Using the properties of constituents and the geometric arrangement similar to those reported by Page, the following values have been selected:

$$E_1 = 7700 \text{ MPa}; \quad E_2 = 8800 \text{ MPa}; \quad \nu_{13} = 0.25; \quad \nu_{21} = 0.29; \quad G_{12} = 1750 \text{ MPa}$$

The results reported by Page provide no information on the stress–strain characteristics. Therefore, the values of the parameters governing the inelastic response have been estimated from other sources. The hardening parameter A has been chosen by examining the results of a set of axial compression tests as reported by Hamid and Drysdale (1980). These results indicate that the axial strain at failure remains within the range of 0.1–0.25%, depending on the orientation of the bed joints relative to the loading direction. By adopting this as a guideline, the value of A was chosen as $A = 0.0004$. It should be noted that, given the

appropriate experimental data, the parameter A may also be defined in terms of a scalar–valued function similar to that employed in Eq. (4). Furthermore, the transition from compaction to dilatancy was assumed to occur at $\eta_c = 0.95\mu^c$, which is typical for a broad class of brittle-plastic materials (e.g. Kupfer et al., 1969; Kotsovos and Newman, 1979). Finally, no information is currently available pertaining to specification of the softening parameter C, Eq. (26). Therefore, some parametric studies have been conducted examining the sensitivity of the global characteristics to the value of this parameter.

The first set of numerical results, as shown in Figs. 4 and 5, pertains to specification of conditions at failure in a series of axial compression/tension tests, performed at different orientation of bed joints relative to the loading direction. Fig. 4a shows the distribution of compressive strength, whereas Fig. 4b presents

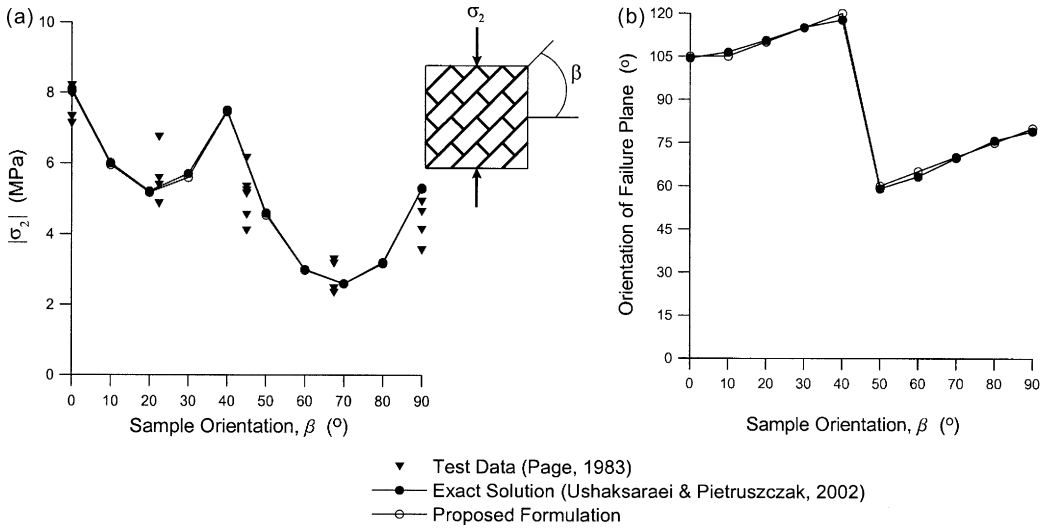

Fig. 4. Variation of uniaxial compressive strength and orientation of failure plane with sample orientation.

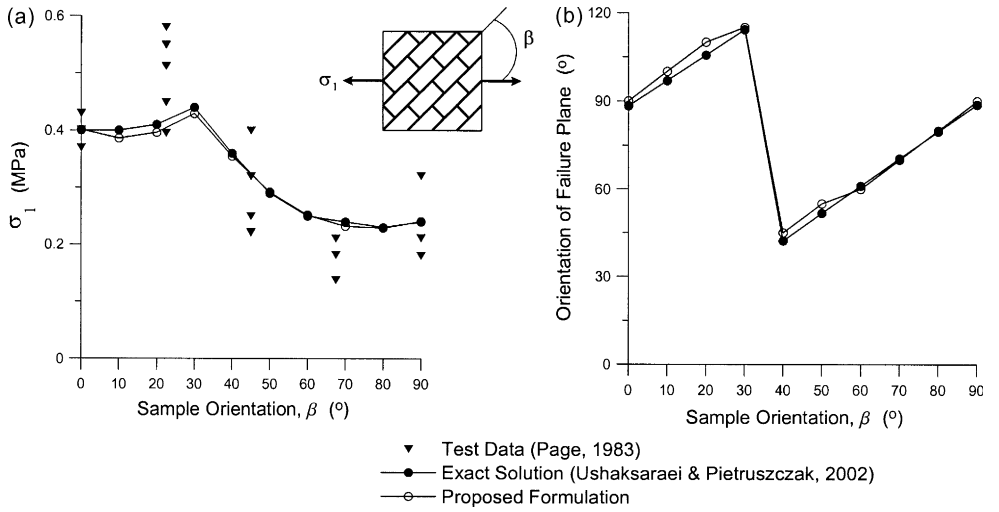

Fig. 5. Variation of uniaxial tensile strength and orientation of failure plane with sample orientation.

the corresponding evolution of the orientation of the localization plane. The results based on the proposed formulation are compared here with the experimental data of Page (1983) as well as with an exact solution obtained by solving a 3D constrained optimization problem, viz. Eq. (5). The primary objective, at this point, is to investigate the accuracy of different integration schemes employed in Eq. (11). Since for all tests considered here the exact solution furnished an in-plane rapture surface, the simulations for the plasticity model have been carried out by employing a 2D sampling rule incorporating a set of 36 uniformly dis-

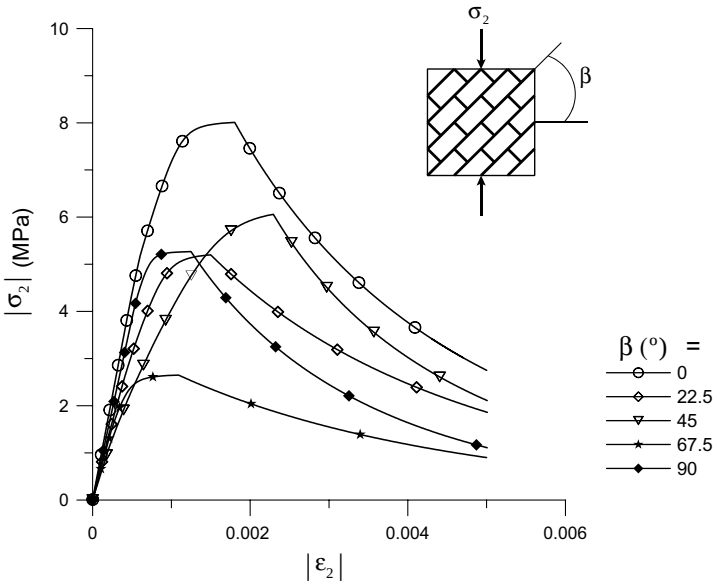

Fig. 6. Stress–strain response in uniaxial compression for different orientations of bed joints.

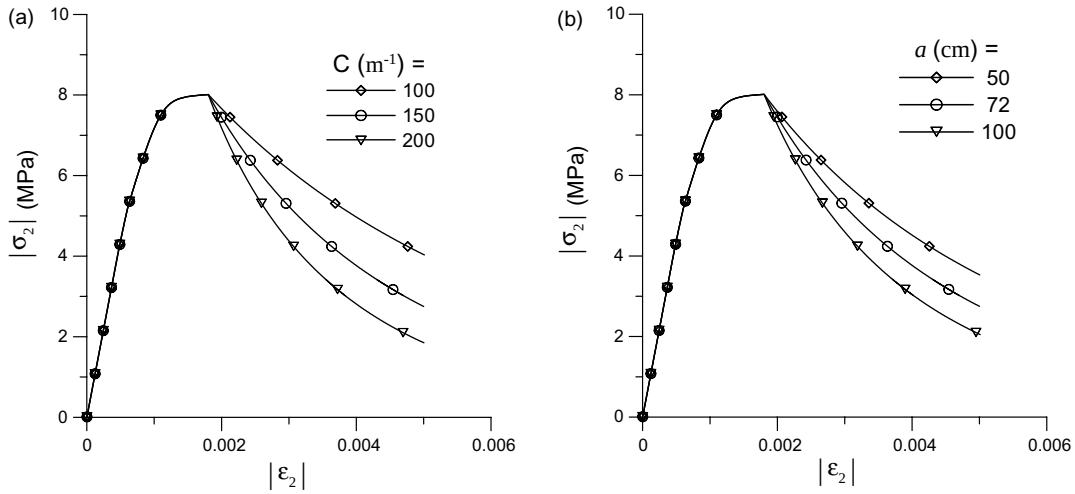

Fig. 7. Influence of the softening parameter, C, and the size of the sample, a, on the response in uniaxial compression ($\beta = 0°$).

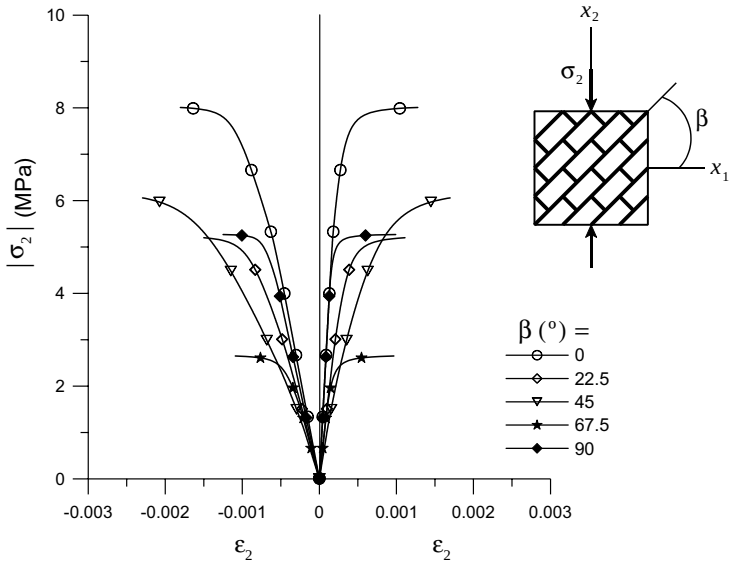

Fig. 8. Stress–strain characteristics in uniaxial compression (in hardening regime).

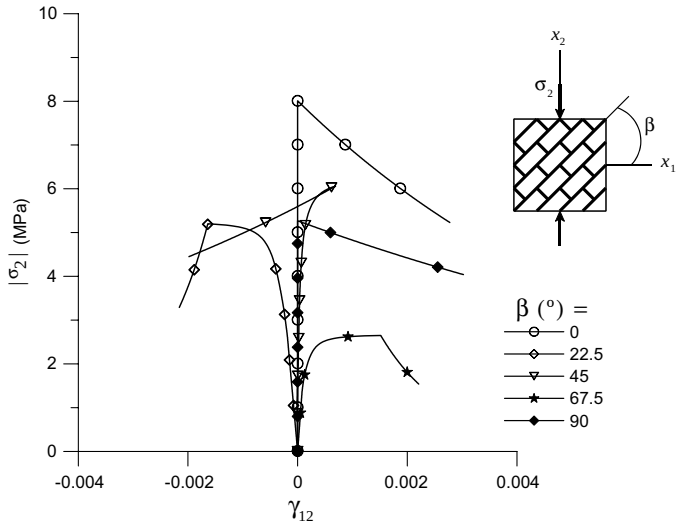

Fig. 9. Evolution of shear strain in uniaxial compression tests.

tributed planes. It is evident that this integration scheme is sufficiently accurate. A similar conclusion can be drawn based on the results reported in Fig. 5, which pertain to a set of axial tension tests.

Examining the results for compression, Fig. 4b, it is evident that for low values of β the failure occurs through formation of macrocracks in the masonry units, in the direction which is in a close proximity of head joints. The minimum strength at $\beta \approx 20^\circ$ is actually associated with the failure along head joints. At $\beta \approx 40^\circ$ there is a transition in the failure mode, i.e. the localization plane is shifted to the region in the vicinity of the bed joints. The minimum, at $\beta \approx 65^\circ$, corresponds to failure of the bed joints. A somewhat

similar trend can be observed in tension, Fig. 5b. Here, for $\beta \leqslant 30°$, the failure of the brickwork is induced by rapture of the head joints, whereas for $\beta > 40°$, the failure occurs in the bed joints. The results of the simulations are, in general, fairly consistent with the data of Page.

Complete mechanical characteristics corresponding to compression regime are shown in a set of subsequent figures. Fig. 6 presents the stress–strain response in uniaxial compression for different orientations of the bed joints. The characteristics shown here include the descending branches, associated with the localized deformation mode. The latter have been computed for a square sample with the in-plane dimension of $a = 0.72$ m, which is representative of the brickwork panel tested by Page. It was assumed that the transition to localized mode commences at $\mu = 0.99\mu^c$, while $C = 150\ \mathrm{m}^{-1}$, Eq. (26). The influence of both parameters C and a on the mechanical response is investigated further in Fig. 7. Here, the simulations are performed for $\beta = 0°$. Evidently, an increase in the value of C results in a steeper descending branch. It is also apparent that the response in the post-localized regime is sensitive to the geometry of the sample. For the same value of C, the average rate of strain–softening increases with the size of the sample, i.e. the value of a.

Fig. 8 presents the variation of vertical compressive stress, in the hardening regime, with both the axial and lateral strains. The trends, as depicted in this figure, are fairly consistent with the experimental data reported by Hamid and Drysdale (1980). For all tests considered here, the deformation mode is, in general, anisotropic; i.e. the change in vertical stress is accompanied by distortion of the sample. This is evidenced in Fig. 9, which presents the evolution of shear strain in samples tested at different orientation relative to the loading direction.

4. Inelastic finite element analysis of a bearing masonry wall subjected to in-plane loading

The proposed constitutive model has been implemented in a finite element code. In what follows, an illustrative example is provided involving a brick masonry wall subjected to in-plane loading under plane stress conditions. The primary objective here is to investigate the evolution of the cracking pattern leading to the collapse of the wall, and to examine a simple reinforcement strategy.

The example involves a masonry wall of a power substation building, typical of those constructed in the Montreal region in Canada (cf. Gocevski et al., 2002). The building, which houses the command panels for

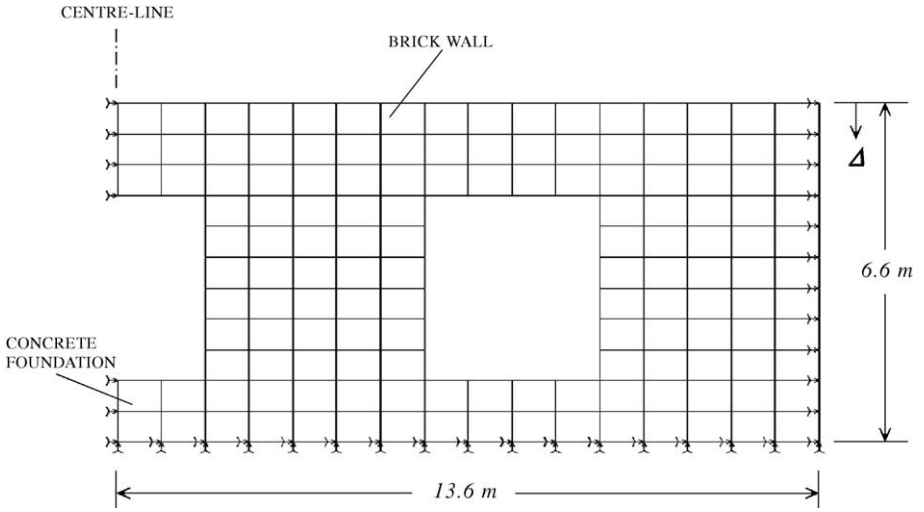

Fig. 10. Finite element discretization of the unreinforced masonry wall.

the substation, is a one-floor structure with the dimensions in the range of 30 m × 30 m. The exterior bearing walls, with the height of approximately 5 m, are made of brick masonry. The part of the structure analyzed here is depicted in Fig. 10. The bearing wall, with the in-plane dimensions of 27.2 m × 5.4 m, has three identical openings with a symmetric arrangement. The wall has a concrete foundation at the base and is reinforced only with concrete beams above the window openings.

The wall was discretized using four-noded rectangular elements with isoparametric formulation and 2 × 2 Gauss quadrature. The concrete beams above the openings were modelled by incorporating 2D beam elements. The material parameters for the brickwork were identical to those used for the numerical simulations discussed in the preceding section. The concrete parts were considered as elastic. Owing to the symmetry in geometry and boundary conditions only a half of the structure was analysed, assuming no horizontal movement along the centre-line of the wall. In addition, the effect of out-of-plane walls was approximated by constraining the horizontal movement along the right-hand boundary (Fig. 10). The loading process consisted of applying uniform vertical displacements along the upper surface, which

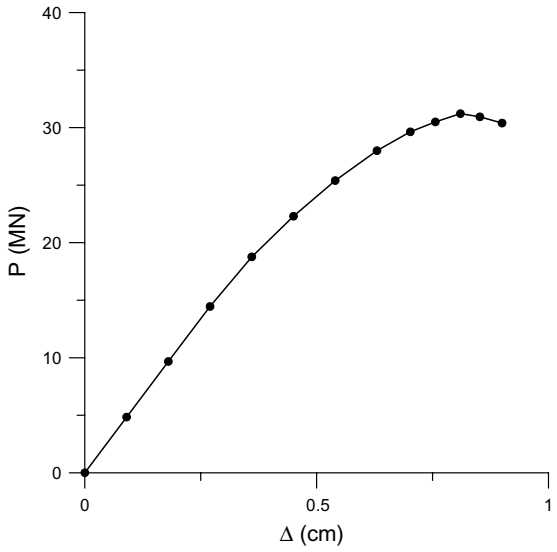

Fig. 11. Global load–displacement response of the unreinforced bearing wall.

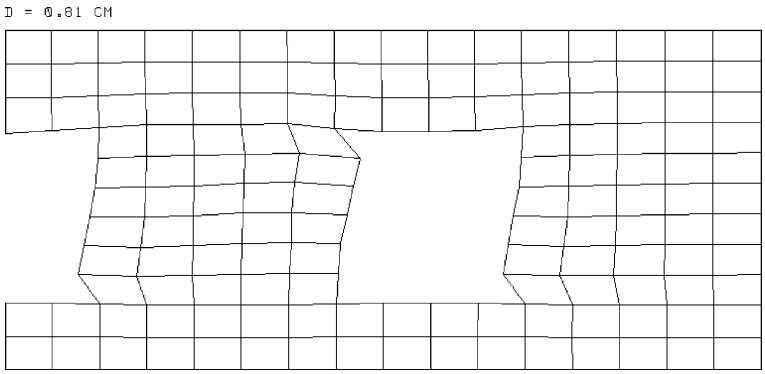

Fig. 12. Distorted mesh of the unreinforced wall at the ultimate load.

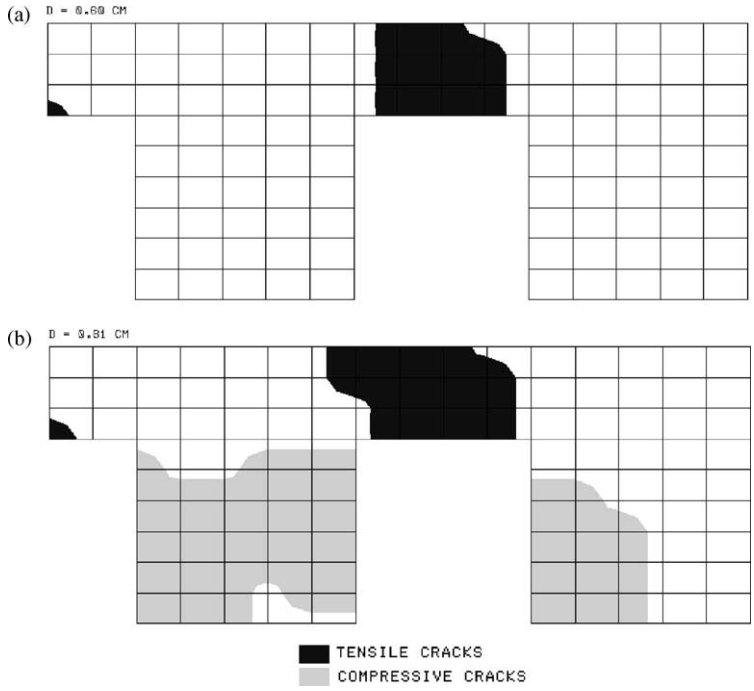

Fig. 13. Evolution of crack patterns in tension and compression regimes for the unreinforced bearing wall.

simulated the load exerted by the roof structure. The problem was solved using the 'tangential stiffness' approach (Owen and Hinton, 1980) and employing a non-symmetric equation solver. Since the analysis incorporating the homogenization procedure, Eq. (19), shows little sensitivity to the discretazation, no explicit mesh convergence study was performed.

The results of the numerical simulations are shown in Figs. 11–15. Fig. 11 presents the global load–displacement characteristic for the wall. The ultimate conditions are reached at the external load of about 30 MN, after which the response becomes unstable. Fig. 12 shows the distorted mesh at the stage preceding the collapse of the wall. It is evident here that significant distortions develop in the neighbourhood of the openings. Fig. 13 shows the evolution of the crack pattern in tension and compression regimes. At the early stages of the deformation process, the tensile cracks form in the region adjacent to the openings and propagate upwards, Fig. 13a. As the load increases further, some compressive cracks develop along the vertical boundaries nearby the openings. Fig. 13b presents the distribution of the damage zones at the ultimate load.

In order to improve the stability of the wall, a simple reinforcement scenario has been considered. This involved the placement of steel bracings behind the critical sections of the brickwork, as indicated in Fig. 14. The horizontal/vertical columns and the cross-braces incorporated W360 × 122 and L152 × 89 × 9.5 cross-sections, respectively, and were modelled using 2D beam elements. Note that the cross-braces were attached to the wall only at the junction between horizontal and vertical columns. The results of numerical simulations are shown in Fig. 15. Fig. 15a presents the load–displacement characteristic, whereas Fig. 15b depicts the pattern of cracking at the external load of about 30 MN (i.e. the ultimate load for the unreinforced system). It is evident that a simple reinforcement strategy employed here is quite efficient. The extent of structural damage is significantly less pronounced and the global characteristic remains in the

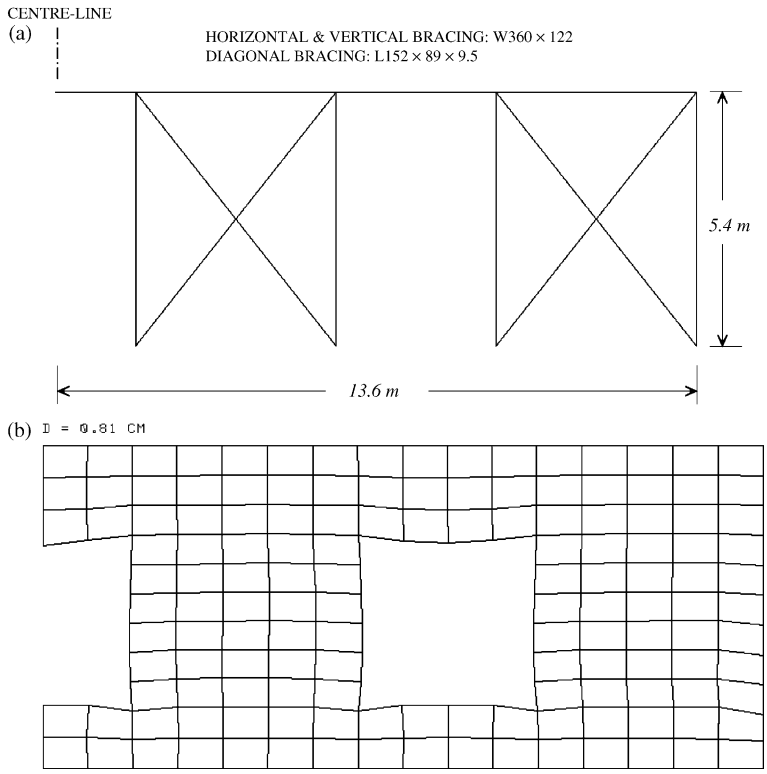

Fig. 14. (a) Details of the steel reinforcement and (b) distorted mesh of the reinforced wall (at the ultimate load for the unreinforced case).

linear range. For the case considered here, the collapse is associated with yielding of the reinforcement and takes place at much higher load intensities.

5. Final remarks

In this work, a continuum framework has been developed for modelling of inelastic behaviour of structural masonry. The formulation incorporates the anisotropic material characteristics and addresses both stages of the deformation process, i.e. those associated with homogeneous as well as localized deformation mode.

The proposed approach depicts the basic trends in the behaviour of structural masonry, in both tension and compression regimes, as evidenced in Section 3. These include a strong sensitivity of mechanical characteristics to the orientation of the sample and the associated evolution of the direction of localization plane. The formulation may be perceived as a pragmatic alternative to the homogenization method. In fact, in the absence of appropriate experimental tests (which are expensive and difficult to perform), the homogenization approach may be implemented to generate a set of data, which can subsequently be used to identify the material parameters/functions involved. Such a methodology, in the context of specification of the conditions at failure, has been employed in Gocevski and Pietruszczak (2001).

The formulation has been implemented in a finite element code and an illustrative numerical example has been provided involving an inelastic analysis of a bearing masonry wall. It needs to be emphasized that the

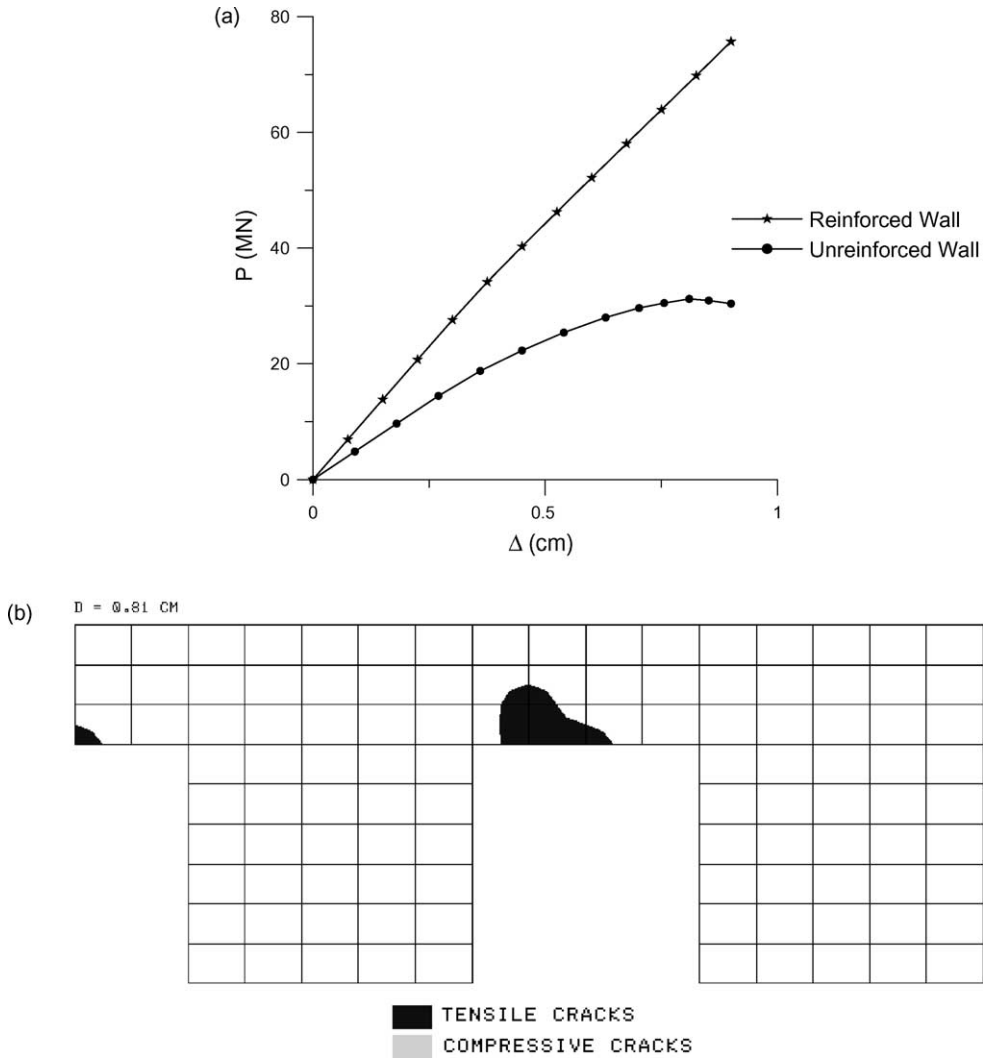

Fig. 15. (a) Global load–displacement response of the reinforced bearing wall and (b) crack patterns at the ultimate load corresponding to the unreinforced case.

previous attempts to model the progressive evolution of failure in masonry structures have been quite scarce. Those which are noticeable, include the work of Lourenco et al. (1998) and Lopez et al. (1999). The present approach is primarily applicable to large-scale masonry structures, as the fundamental assumption employed here is that of the macrohomogeneity of the medium.

References

Anthoine, A., 1995. Derivation of in-plane elastic characteristics of masonry through homogenization theory. Int. J. Solids Struct. 32 (2), 137–163.

Anthoine, A., 1997. Homogenisation of periodic masonry: plane stress, generalized plane strain or 3D modelling? Commun. Numer. Meth. Eng. 13, 319–326.

Gocevski, V., Pietruszczak, S., 2001. Seismic analysis of brick masonry walls of the Beauharnois powerhouse in Quebec, Canada. In: Computer Methods in Structural Masonry—5. Computers & Geotechnics Ltd, pp. 141–148.

Gocevski, V., Pietruszczak, S., Ushaksaraei, R., 2002. Seismic analysis of brick masonry walls of a power substation building. In: Numerical Models in Geomechanics, NUMOG VIII. AA Balkema Publ, pp. 643–649.

Hamid, A.A., Drysdale, R.G., 1980. Concrete masonry under combined shear and compression along the mortar joints. ACI Struct. J. 77 (5), 14–320.

Kotsovos, M.D., Newman, J.B., 1979. A mathematical description of the deformation behaviour of concrete under complex loading. Mag. Concr. Res. 31 (107), 77–90.

Kupfer, H., Hilsdorf, H.K., Rusch, H., 1969. Behaviour of concrete under biaxial stress. Proc. Am. Concr. Inst. 66 (8), 656–666.

Lopez, J., Oller, S., Onate, E., Lubliner, J., 1999. A homogeneous constitutive model for masonry. Int. J. Numer. Meth. Eng. 46, 1651–1671.

Lourenco, P.B., Rots, J.G., Blaauwendraad, J., 1998. Continuum model for masonry: parameter estimation and validation. J. Struct. Eng. ASCE 124 (6), 642–652.

Lourenco, P.B., Zucchini, A., 2001. A homogenization model for stretcher bond masonry. In: Computer Methods in Structural Masonry—5. Computers & Geotechnics Ltd, pp. 60–67.

Maier, G., Papa, E., Nappi, A., 1991. On damage and failure of unit masonry. In: Experimental and Numerical Methods in Earthquake Engineering. AA Balkema Publ, pp. 223–245.

Masiani, R., Trovalusci, P., 1996. Cauchy and Cosserat materials as continuum models of brick masonry. Meccanica 31, 421–432.

Owen, D.R.J., Hinton, E., 1980. Finite Elements in Plasticity: Theory and Practice. Pineridge Press, Swansea.

Page, A.W., 1983. The strength of brick masonry under biaxial tension–compression. Int. J. Masonry Constr. 3 (1), 26–31.

Pande, G.N., Sharma, K.G., 1983. Multi-laminate model of clays—a numerical evaluation of the influence of rotation of the principal stress axes. Int. J. Numer. Anal. Meth. Geomech. 7, 397–418.

Pande, G.N., Liang, J.X., Middleton, J., 1989. Equivalent elastic moduli for brick masonry. Comput. Geotech. 8, 243–265.

Pietruszczak, S., 1999. On homogeneous and localized deformation in water-infiltrated soils. Int. J. Damage Mech. 8, 233–253.

Pietruszczak, S., Mroz, Z., 2001. On failure criteria for anisotropic cohesive-frictional materials. Int. J. Numer. Anal. Meth. Geomech. 25, 509–524.

Pietruszczak, S., Niu, X., 1992. A mathematical description of macroscopic behaviour of brick masonry. Int. J. Solids Struct. 29 (5), 531–546.

Pietruszczak, S., Pande, G.N., 1987. Multi-laminate framework of soil models—plasticity formulation. Int. J. Numer. Anal. Meth. Geomech. 11, 651–658.

Sulem, J., Muhlhaus, H.B., 1997. A continuum model for periodic two-dimensional block structures. Mech. Coh. Frict. Mater. 2, 31–46.

Urbanski, A., Szarlinski, J., Kordecki, Z., 1995. Finite element modelling of the behaviour of masonry walls and columns by homogenization approach. In: Computer Methods in Structural Masonry—3. B & J Intern, pp. 32–41.

Ushaksaraei, R., Pietruszczak, S., 2002. Failure criterion for structural masonry based on critical plane approach. J. Eng. Mech. ASCE 128 (7), 769–778.